Composites: Part B 50 (2013) 325–332

Contents lists available at SciVerse ScienceDirect

Composites: Part B

journal homepage: www.elsevier.com/locate/compositesb

Impactor diameter effect on low velocity impact response of woven glass epoxy composite plates

Bulent Murat Icten [a,*], Binnur Goren Kıral [a], Mehmet Emin Deniz [b]

[a] Department of Mechanical Engineering, Dokuz Eylul University, 35397 Izmir, Turkey
[b] Department of Mechanical Engineering, Batman University, 72100 Batman, Turkey

ARTICLE INFO

Article history:
Received 2 July 2012
Received in revised form 19 September 2012
Accepted 21 February 2013
Available online 4 March 2013

Keywords:
A. Polymer–matrix composites (PMCs)
B. Impact behavior
C. Finite element analysis (FEA)
D. Mechanical testing

ABSTRACT

In this study, the effect of impactor diameter on the impact response of woven glass–epoxy laminates has been investigated. Impact tests were performed by using Fractovis Plus test machine with four different impactor nose diameters as 12.7, 20.0, 25.4 and 31.8 mm. Specimens were impacted at various impact energies ranging from 5 J to perforation thresholds of the composite at room temperature. Variation of the impact characteristics such as the maximum contact load, maximum deflection, maximum contact time and absorbed energy versus impact energy are investigated. Results indicated that the projectile diameter highly affects the impact and Compression After Impact (CAI) response of composite materials.

1. Introduction

Fiber reinforced polymer matrix composite materials are widely used in many applications such as aircraft, marine and automotive parts due to their high specific strength and stiffness properties. However, their behavior under impact loading is one of the major concerns, since impacts may occur during manufacture, normal operations, maintenance and so on. Many experimental and numerical studies have been carried out to understand the impact behavior of composites and they are presented in review articles [1–3].

Woven fabric composites are being considered for high performance applications. Due to the interlacing of fiber tows in two directions, woven fabric composites offer better impact resistance and smaller delamination area as compared to unidirectional composites [4,5]. There have been many studies on impact response of woven composite plates [4–8].

In many studies, hemispherical impactor, generally 12.7 mm (0.5 in.) diameter has been used. However, different impactor shapes cause different damage mechanisms and areas in composite structures. That's why it is important to examine the effect of the impactor shapes on the damage process. Various studies for both low and high velocity impact considering the effect of impactor shape, have been carried out recently [9–15]. Mitrevski et al. [9] investigated the effect of impactor shape on the impact response of thin woven carbon/epoxy laminates experimentally. The experimental studies were carried out using 12 mm diameter hemispherical, ogival and conical impactors at initial impact energies of 4 J and 6 J. They pointed out the important contribution of impactor shape on the resulting damage and response of composite laminates. Mitrevski et al. [10] investigated the post-impact damage properties of composite laminates impacted by various impactor shapes. After impacting thin woven carbon/epoxy laminates using hemispherical, ogival and conical steel impactors all 12 mm in diameter using a drop weight test rig, various post-impact analysis techniques were employed, such as non-destructive inspection (NDI) and microscopy to assess the effect of impactor shape on the resulting damage. The simultaneous effect of impactor shape and biaxial preload on the impact response of thin glass fiber reinforced polyester laminates were investigated by Mitrevski et al. [11]. Specimens were impacted at initial impact energies of 4 J and 6 J using steel flat, hemispherical, ogival and conical impactors, all 12 mm in diameter. It was found that for the applied levels of preload, there were no significant effects on the impact response using the various impactor shapes. The only notable effect was on the specimens impacted by the conical impactor at an initial impact energy of 4 J.

Ulven et al. [12] examined the effect of the projectile geometry on the damage propagation and evolution during ballistic impact normal to carbon/epoxy composite panels. They studied the perforation mechanism, ballistic limit, and damage evolution and performed a series of ballistic high velocity impact tests for different projectile geometries, namely, hemispherical, conical, fragment simulating and flat. Wen [13,14] examined the penetration and perforation of FRP laminates using flat-faced, hemispherical-ended, conical-tip, and truncated-cone-nose projectiles in high

* Corresponding author. Tel.: +90 232 3019220; fax: +90 232 3019204.
E-mail address: bulent.icten@deu.edu.tr (B.M. Icten).

1359-8368/$ - see front matter © 2013 Elsevier Ltd. All rights reserved.
http://dx.doi.org/10.1016/j.compositesb.2013.02.024

Table 1
Mechanical properties of woven glass–epoxy composite used in this study.

Symbol	Explanation	Standard	Magnitude
E_1	Modulus of elasticity in 1st direction		22.32 GPa
X_{1t}	Tensile strength in 1st direction	ASTM D3039	406 MPa
ν_{12}	Poisson's ratio		0.16
E_2	Modulus of elasticity 2nd direction	ASTM	21.3 GPa
X_{2t}	Tensile strength in 2nd direction	D3039	346 MPa
X_{1c}	Compressive strength in 1st direction	ASTM D3410	233 MPa
X_{2c}	Compressive strength in 2nd direction	ASTM D3410	210 MPa
G_{12}	Shear modulus	ASTM	3080 MPa
S	Shear strength	D7078	65 MPa

velocity impact. He developed analytical equations for predicting the penetration and perforation for each shape of projectile. In an experimental work, Tan and Khoo [15] investigated the response of flexible laminates comprising [0°/90°] extended chain polyethylene filaments embedded in a thermoplastic resin to ballistic impacts by projectiles of various geometries, namely, flat-ended, hemispherical, ogival and conical projectiles. They showed that the region of the specimens affected by the projectiles appears to increase in size instead of becoming more localized at higher impact velocities as often reported for most ballistic impact events, including the ballistic perforation of woven fabric. They emphasized that flexible laminates are more effective in dissipating energy than woven fabric in the application of flexible armor.

The present study aims to examine the effect of impactor diameter on the impact response of woven glass–epoxy laminates. Impact tests were performed using Fractovis Plus test machine with four different impactor diameters. Specimens were single impacted at varied impact energies ranging from 5 J to perforation thresholds of the composite at room temperature. The effects of the impactor size on the maximum contact force, maximum deflection, maximum contact time and absorbed energy versus impact energy were investigated. To determine the compressive loading capacity of the impacted specimen, CAI tests were conducted.

2. Experimental part

Composite material was manufactured by vacuum assisted resin infusion method using six layers of plain weave glass fabric each of 500 g/m^2 and an epoxy resin. Curing was performed on specially designed heating table at 90 °C for 2 h. The specimens were trimmed from the composite plate having the dimensions of 150 × 150 mm^2. The nominal thickness of the specimens and the fiber volume fraction of the composite were measured as 2.50 mm and 65%, respectively.

The plain weave patterns with 22 yarns/10 cm in direction 1 and 19 yarns/10 cm in direction 2 were used as reinforcement. Because of the closer yarn numbers in directions, similar mechanical properties are obtained as expected along the principal directions. The material properties of the composite and the related ASTM standards are shown in Table 1.

Impact tests were performed for various impact energies ranging from 5 J to the energy levels which perforation occurred using Fractovis Plus drop weight impact test machine. The base of the machine is designed as an environmental chamber as well as the pneumatic clamping device. The inner diameter of the clamping apparatus of the impact machine was 76 mm (Fig. 1). In the upper part of the machine, the mass of the dropping tool that includes the weight box for adding mass in and the striker was approximately 5 kg. The striker is composed of the rod, force transducer and the impactor nose. The force transducer having a capacity of 22.24 kN is mounted between the steel rod and the impactor nose.

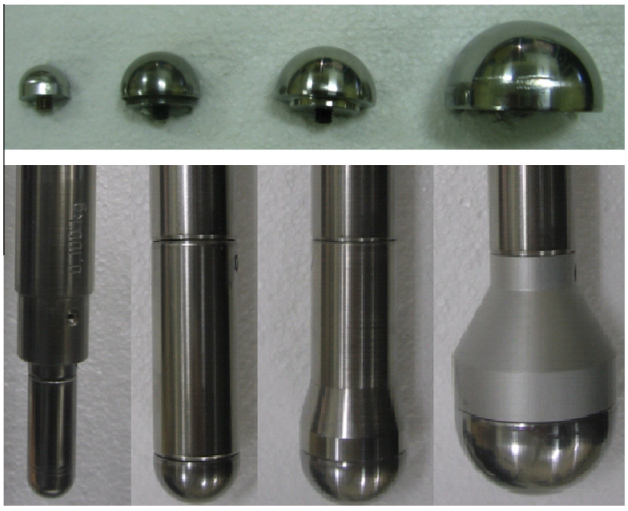

Fig. 2. The impactor nose having diameter of 12.7 mm, 20 mm, 25.4 mm and 38.1 mm.

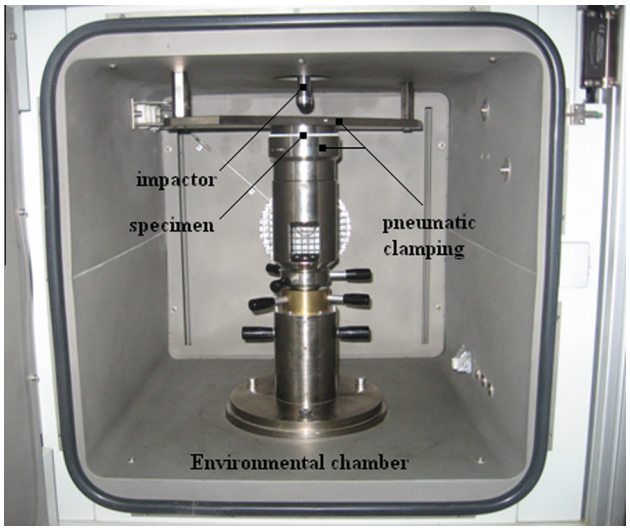

Fig. 1. Impact test fixture.

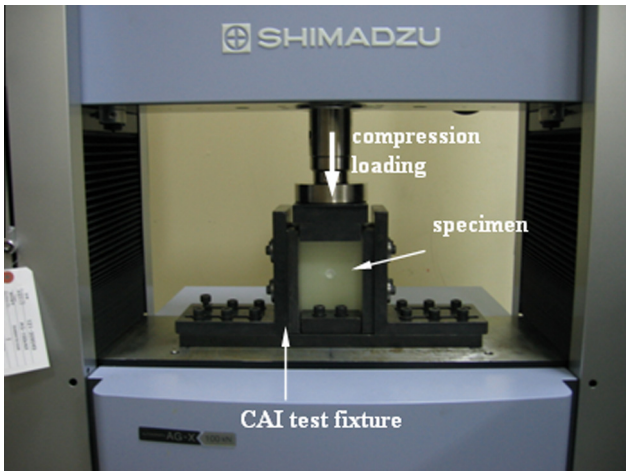

Fig. 3. Compression After Impact (CAI) test system.

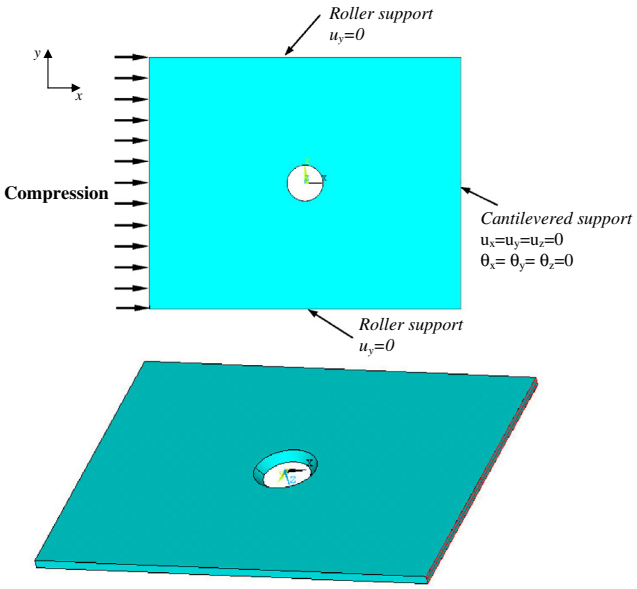

Fig. 4. Three-dimensional solid model of the impacted specimen.

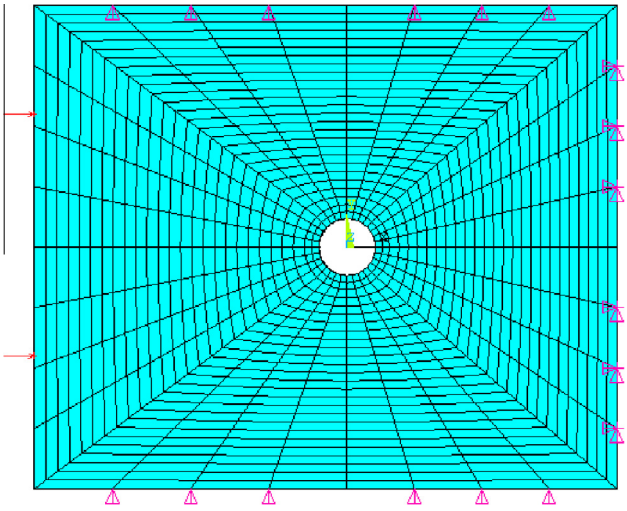

Fig. 5. Finite element model of the impacted specimen.

A software based on Newton's second law and kinematics converted the time–force history taken from the force transducer to the velocity and displacement histories. Four different impactor nose diameters were used. The impactors used in the study are seen in Fig. 2.

The Compression After Impact (CAI) test fixture shown in Fig. 3 was used to find the compression strength of the impacted specimen. According to ASTM D 7137, impacted specimens are trimmed to the dimension of CAI specimens, with a height of 150-mm and a width of 100-mm. The CAI tests were performed at room temperature using Shimadzu AG tensile–compression test machine with 100 kN loading capacity. The CAI strength of the specimen is calculated by,

$$\sigma_{CAI} = \frac{F_{\max}}{bt}$$

where $F_{\max}$, b and t denote the maximum compression force, width and thickness of the specimen, respectively. The maximum compression force is obtained from the force–displacement curves.

3. Numerical part

Finite element analyses simulating the CAI test procedure of impacted specimens were performed using ANSYS v11 commercial software in the numerical part of the study. APDL (ANSYS Parametric Design Language) code was developed to determine the failure loads of delaminated plates having different delamination configurations. Eight-noded layered solid elements (SOLID46) for the impacted composite plate were used. Fig. 4 shows the boundary conditions of specimens to simulate the conditions of Compression After Impact. As shown in the figure, the specimen is subjected to compression load as one of the other edges are cantilevered, which restrict the translation and rotation while the other two edges have roller support. According to the type of the damage, cylindrical and conical delaminations or holes were generated in the three-dimensional finite element models. Finite element model having the hole is shown in Fig. 5. In order to obtain accurate results, finer mesh was selected around the delamination and the hole.

The failure analyses in this study were based on the assumption that the material is linear elastic. Tsai-Wu criterion was employed to check whether failure has occurred. If no failure was detected, the load was incremented. In the finite element analyses, the first

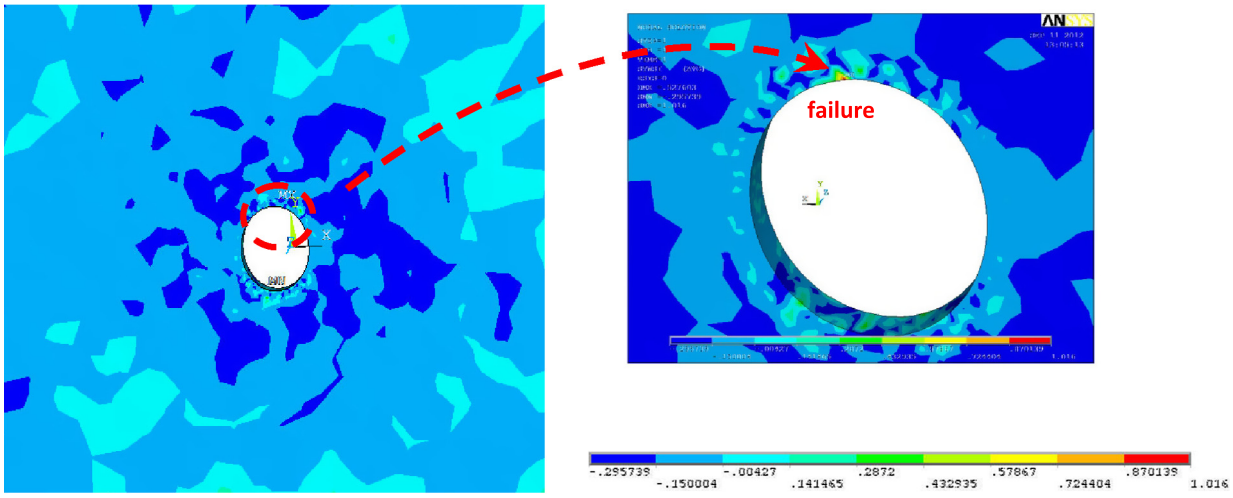

Fig. 6. Tsai-Wu Index distribution for an impacted composite plate having a hole.

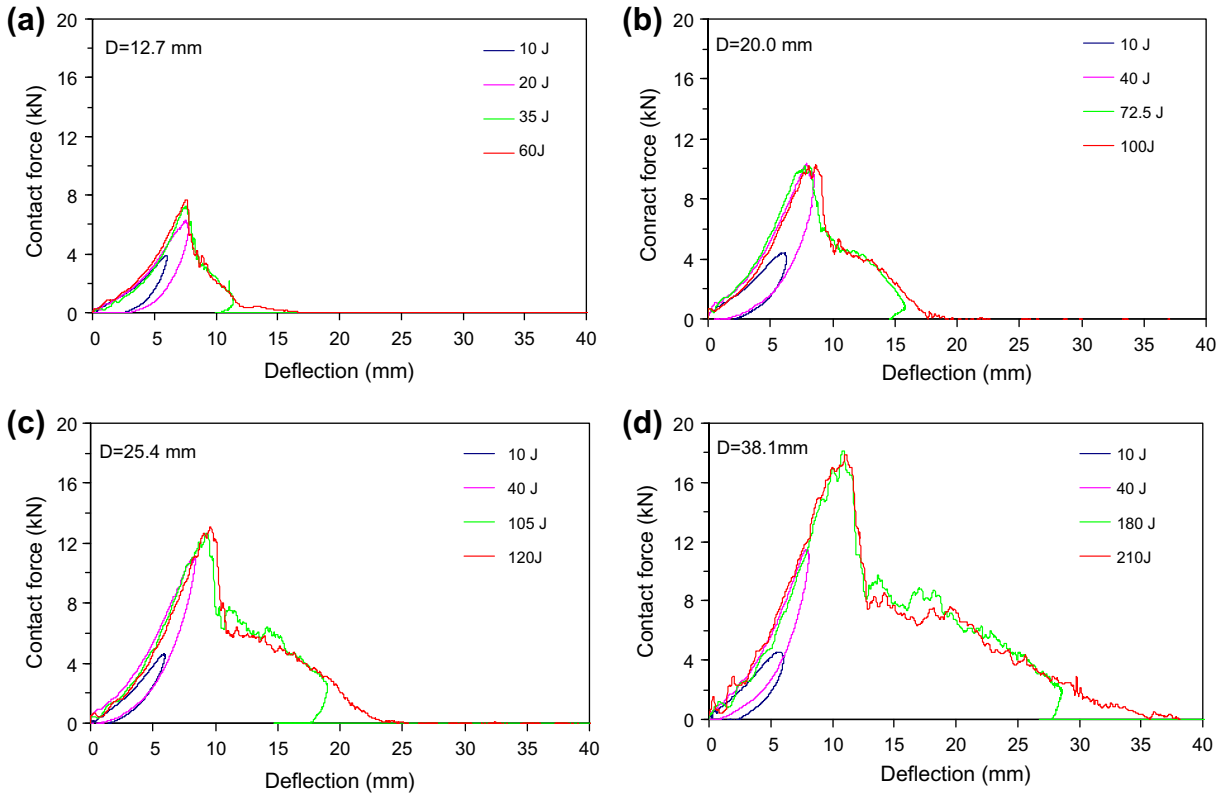

Fig. 7. Contact force–deflection curves of the experiment performed with the impactor nose having: (a) 12.7 mm, (b) 20 mm, (c) 25.4 mm, and (d) 38.1 mm, diameter.

failure loads for impacted composite plates were determined. Fig. 6 shows the impacted laminated composite plates damaged.

4. Results and discussion

Variation of the contact force between the impactor and specimen versus deflection of the specimen at contact point for some critical impact energy values are given in Fig. 7. As seen from the figure, three different cases are presented. The first one is the rebounding, which the curves for 10 J and 20 J in Fig. 7a exemplify this case. Two different tendencies are observed in the case of rebounding. The contact force at the beginning of the curve increases with increasing deflection up to the maximum value for both. Thereafter, the deflection and the contact force values decrease in the first tendency. In higher impact energy levels, the contact force reaches the peak value. Afterwards, the contact force values decrease with increasing the deflection up to the maximum deflection value. Following this, the contact force again decreases with increasing deflection values (Fig. 7b – 40 J). The deflection–contact force curves in both rebounding cases are closed.

Increase in the impact energy causes more severe failure resulting in decreasing contact force with increasing deflection. Finally, the curve does not go toward to the origin but towards the horizontal axis (Fig. 7b – 72.5 J). This is penetration. Increase in the impact energy causes the perforation of the specimen. Excessive energy is spent by friction between the impactor nose and surface of the hole in the perforated specimen (Fig. 7a – 60 J).

The absorbed energy by the specimen for failure is calculated from the closed area of curves for rebounding and penetration. For the perforation case, the absorbed energy is calculated from the total area between the curve and horizontal axis minus the area consumed for friction [16].

In the light of the information mentioned above, Fig. 7 shows that the absorbed energy values for penetration and perforation cases increase with increasing diameter. In those cases, the maximum contact force and the maximum deflection values also increase with increasing diameter of the hemispherical nose.

The contact force–deflection curves obtained from the tests with four impact nose diameters for 10 J are given in Fig. 8. The stiffness value which is determined by the slope of the inclined section of contact force–deflection curve increases with increasing diameter. For rebounding case, the intersection point of the curve to the horizontal axis may give information about the depth of the mark of the impactor at the contact point. The mark depth of the specimen decreases with increasing impactor nose diameter. The mark depth of the specimen is nearly zero for the impact with 38.1 mm diameter impactor nose. It is also obviously observed from Fig. 8 that the absorbed energy by the specimen is higher in the tests performed with the impactor having a smaller diameter.

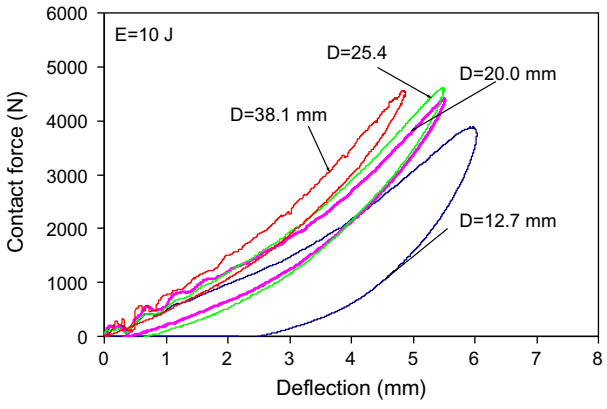

Fig. 8. Comparison of the contact force–deflection curves with different nose diameter at the same impact energies.

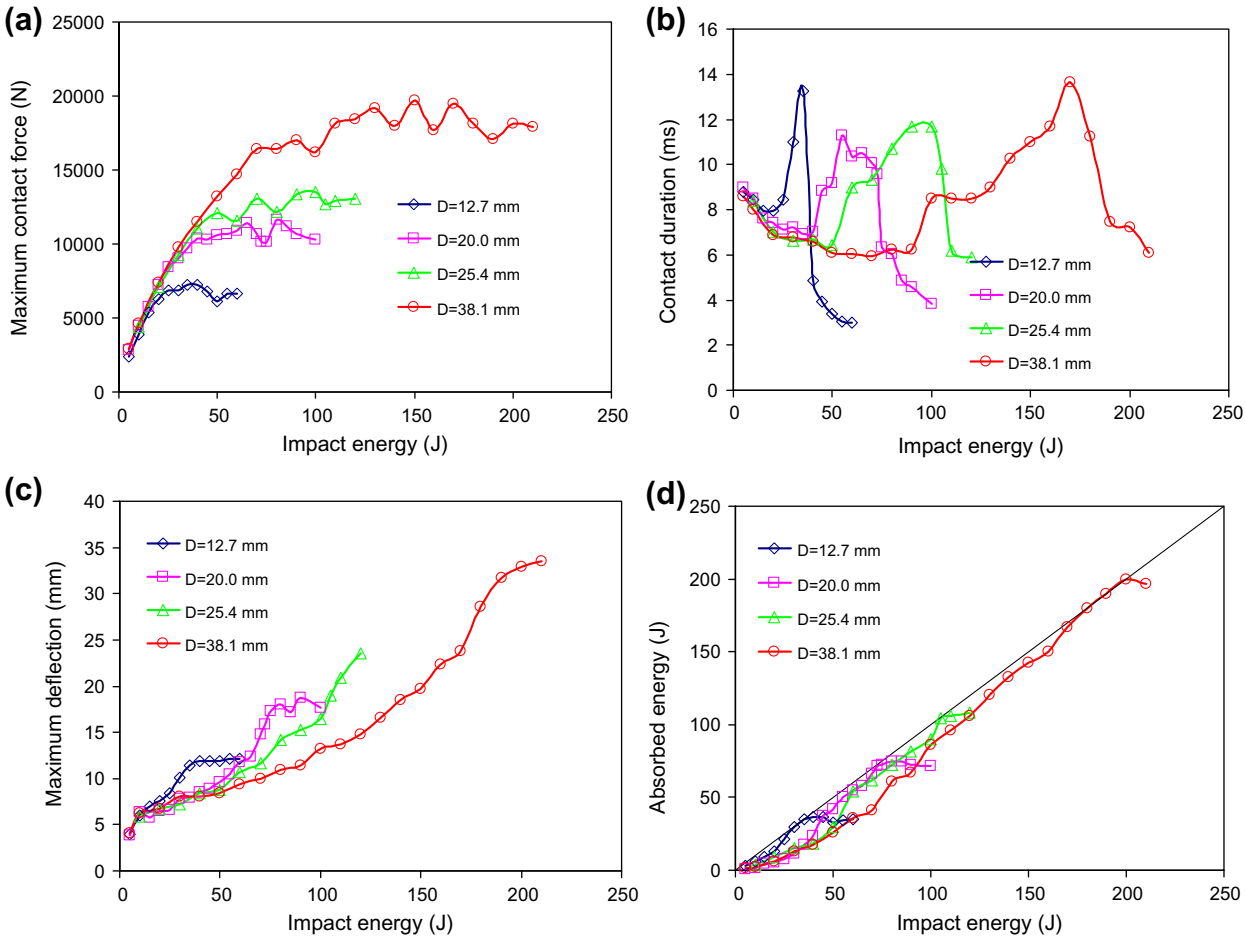

Fig. 9. Impact energy versus: (a) maximum contact force, (b) contact duration, (c) maximum deflection, and (d) absorbed energy data of the woven $[0/90]_6$ composite impacted with various impactor nose diameter as 12.7 mm, 20.0 mm, 25.4 mm and 38.1 mm.

The maximum contact force, contact duration, maximum deflection and absorbed energy values for all experiments conducted is given in Fig. 9. As seen in Fig. 9a, the peak contact force increases with the increase of impact energy, up to 70 J for the impactor diameter of 38.1 mm. Then, it reaches a maximum value and remains nearly constant at impact energies higher than 70 J. Actually up to this impact energy, failure is seen in the composite in the manner of the matrix cracking and fiber breakages. This impact energy level is the threshold to the serious failure such as through-thickness fiber breakages. For the tests performed with the other impactor diameters, through-thickness failure occurs at lower impact energy levels. However, the general tendency of the maximum contact force versus impact energy is similar. It is also seen from Fig. 9a that in the case using the impactor with larger diameter, the maximum contact force is higher at the same impact energy levels.

As seen in Fig. 9b, using the impactor with a diameter of 38.1 mm, the contact time decreases with increasing impact energy up to the 70 J. After this energy level, the contact duration increases with increasing impact energy and reaches the maximum value right before the perforation threshold. Once perforation takes place, a sudden drop appears in contact duration since the impactor nose is no longer in contact with the composite. The general shape of the contact time versus the impact energy curves is similar for the tests performed with the various impactor diameters. Depending on the impactor nose diameter, the curve is narrower or wider as seen in Fig. 9b. The macro failure zones such as penetration and perforation can be clearly seen in this figure.

Deflection increases with increasing impact energy values for the tests with different impactor diameters. The general shape of the impact energy versus deflection curves is similar. However, the curve gets wider with the impactors of larger diameter (Fig. 9c).

Variation of the absorbed energy versus impact energy called as energy profile diagram is shown in Fig. 9d. The energy profile is a useful graphical method for understanding the overall energy absorption process in an impact event. The pure elastic limit, penetration and perforation threshold can be characterized by using this method. For example, the end of the linearly increasing data of the tests performed by the impactor having a diameter of 38.1 mm (impact energy of 70 J) shown in Fig. 9d is the pure elastic limit. The diagonal line in the impact energy and absorbed energy diagram represents the equal energy line. Penetration threshold is the first test data meeting on the equal energy line. Impact energy of 180 J is the penetration threshold of the example case (Fig. 9d and impactor diameter of 38.1 mm). End of the penetration is the perforation threshold. Beyond this threshold, the absorbed energy does not change with increasing impact energy. The perforation threshold of the example case is 200 J. In some cases, defining the penetration threshold is very difficult. In this situation, penetration and perforation threshold can be taken as the same value.

The excessive energy is retained in the impactor and used for rebound of the impactor from the specimen at the end of test. The excessive energy can be seen from Fig. 9d as the vertical difference between the equal energy line and the data points. As can be seen from this figure, penetration and perforation thresholds increase

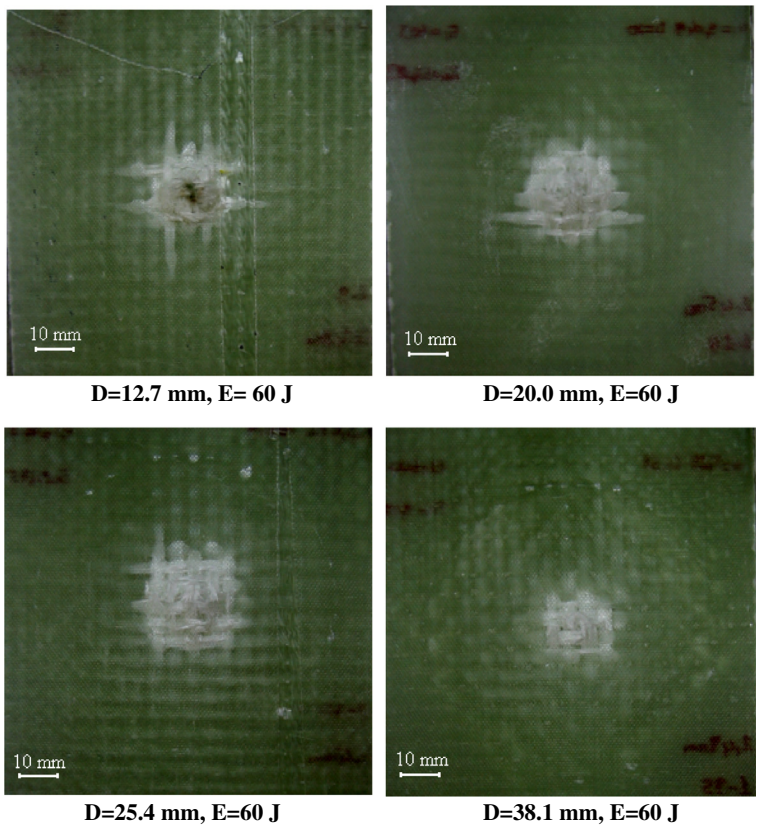

Fig. 10. Photos of the back face of the specimens impacted at 60 J with impactor diameter of 12.7 mm, 20 mm, 25.4 mm and 38.1 mm (focused around the failure).

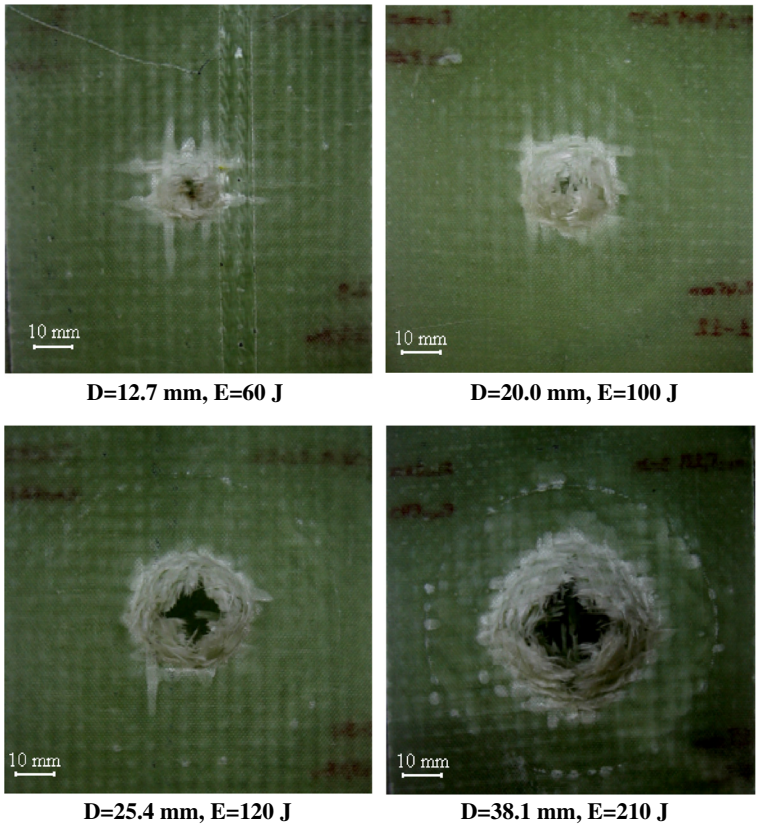

Fig. 11. Photos of the back face of the perforated specimens impacted at various impact energies with impactor diameter of 12.7 mm, 20 mm, 25.4 mm and 38.1 mm (focused around the failure).

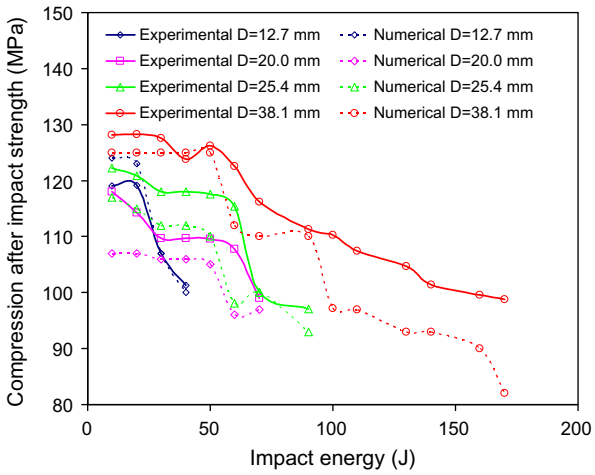

Fig. 12. The experimental and numerical results of CAI strength.

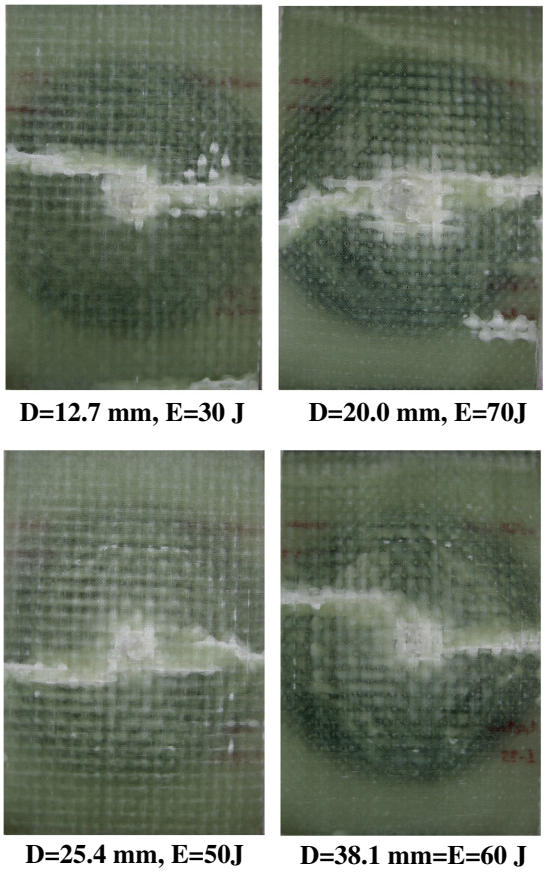

Fig. 13. The photos of CAI specimen.

with increasing impactor diameter. In addition, for low impact energy, i.e. up to the penetration threshold of the case with the impactor diameter of 12.7 mm, absorbed energy decreases with increasing impactor diameter. The example contact force- deflection curves from this region are mentioned above and given in Fig. 7.

The photos focused on the impacted point taken from the non-impacted face of the composite are given in Fig. 10. All composites shown in this figure are impacted at 60 J with the impactor having diameters of 12.7 mm, 20.0 mm, 25.4 mm and 38.1 mm. As can be seen from the figure, the impactor diameter highly affects failure. As the composite impacted with the 12.7 mm impactor is perforated, the composite impacted with 38.1 mm impactor is not perforated and the failure area is small compared to other impactor diameters. The photos of the perforated specimens impacted with various impactor diameter and impact energies are given in Fig. 11.

The experimental and numerical results of the CAI strength of the composite impacted with the impactor having diameters of 12.7 mm, 20.0 mm, 25.4 mm and 38.1 mm are shown in Fig. 12. The analysis was performed for only the specimens which have not been perforated. For all impactor diameter cases the CAI strength of the composites decrease with increasing impact energy. Larger failure area as a result of the higher impact energy reduces the CAI strength. Generally, CAI strength increases with increasing impactor diameter at the same impact energy levels. It is seen that the experimental and numerical results are compatible.

The difference of CAI strength between the non-impacted case and at the end of the non-perforated case is 13% for the composite impacted with 12.7 mm impactor nose diameter. This difference increases with increasing impactor diameter. Some of the CAI photos of the specimen impacted with 12.7 mm, 20 mm, 25.4 mm and 38.1 mm diameter impactor noses are given in Fig. 13.

5. Conclusions

In this study, the impact and the compressive after impact response of woven glass–epoxy composite plates were investigated. The hemispherical impactor nose with diameters of 12.7 mm, 20.0 mm, 25.4 mm and 38.1 mm were selected. The impactor mass was approximately 5 kg. The impact tests were continued up to the perforation of the specimens. After impact tests, compression tests were performed. From the experimental and numerical studies, the following conclusions can be drawn:

(1) The stiffness value, which is determined as the slope of the inclined section of contact force–deflection curve increases with increasing impactor diameter.
(2) For the same impact energies, the maximum contact force is higher for higher impactor diameter.
(3) Penetration and perforation thresholds increase with increasing impactor diameter.
(4) For low impact energies, i.e. up to the penetration threshold of the case with the impactor diameter of 12.7 mm, the absorbed energy decreases with increasing impactor diameter.
(5) For all impactor diameter cases, CAI strength of the composites decreases with increasing impact energy.
(6) Generally, CAI strength increases with increasing impactor diameter at the same impact energy level. The difference of CAI strength between the non-impacted case and at the end of the non-perforated case increases with increasing impactor diameter.

Acknowledgement

The authors are greatly indebted to the TUBITAK Research Foundation for providing financial support (Project Number: 107M591).

References

[1] Abrate S. Impact on laminated composite materials. Appl Mech Rev 1991;44:155–90.
[2] Abrate S. Impact on laminated composite materials: recent advances. Appl Mech Rev 1994;47:517–44.
[3] Cantwell WJ, Morton J. The impact resistance of composite materials – a review. Composites 1991;22:347–62.

[4] Hosur MV, Adya M, Alexander J, Jeelani S. Studies on impact damage resistance of affordable stitched woven carbon/epoxy composite laminates. J Reinf Plast Compos 2003;22:927–52.
[5] Icten BM, Karakuzu R. Effects of weaving density and curing pressure on impact behavior of woven composite plates. J Reinf Plast Compos 2008;27:1083–92.
[6] Baucom JN, Zikry MA. Low-velocity impact damage progression in woven e-glass composite systems. Compos Part A – Appl Sci 2005;36:658–64.
[7] Naik NK, Borade SV, Arya H, Sailendra M, Prabhu SV. Experimental studies on impact behaviour of woven fabric composites: effect of impact parameters. J Reinf Plast Compos 2002;21:1347–62.
[8] Naik NK, Sailendra M, Chandrasekher Y. Polymer matrix woven fabric composites subjected to low velocity impact: Part III – effect of incident impact velocity and impactor mass. J Reinf Plast Compos 2001;20:720–43.
[9] Mitrevski T, Marshall IH, Thomson R, Jones R, Whittingham B. The effect of impactor shape on the impact response of composite laminates. Compos Struct 2005;67:139–48.
[10] Mitrevski T, Marshall IH, Thomson R. The influence of impactor shape on the damage to composite laminates. Compos Struct 2006;76:116–22.
[11] Mitrevski T, Marshall IH, Thomson R, Jones R. Low-velocity impacts on preloaded GFRP specimens with various impactor shapes. Compos Struct 2006;76:209–17.
[12] Ulven C, Vaidya UK, Hosur MV. Effect of projectile shape during ballistic perforation of VARTM carbon/epoxy composite panels. Compos Struct 2003;61:143–50.
[13] Wen HM. Predicting the penetration and perforation of FRP laminates struck normally by projectiles with different nose shapes. Compos Struct 2000;49:321–9.
[14] Wen HM. Penetration and perforation of thick FRP laminates. Compos Sci Technol 2001;61:1163–72.
[15] Tan VBC, Khoo KJL. Perforation of flexible laminates by projectiles of different geometry. Int J Imp Eng 2005;31:793–810.
[16] Coppens GJ. Effects of three-dimensional geometry on penetration and perforation resistance. M.Sc. Thesis, Michigan State University; 2004.